Research in Astron. Astrophys. **2012** Vol. **12** No. **5**, 551–562
http://www.raa-journal.org *http://www.iop.org/journals/raa*

Research in Astronomy and Astrophysics

Periodic orbits around areostationary points in the Martian gravity field *

Xiao-Dong Liu, Hexi Baoyin and Xing-Rui Ma

School of Aerospace, Tsinghua University, 100084 Beijing, China;
liu-xd08@mails.tsinghua.edu.cn

Received 2011 October 11; accepted 2012 January 18

Abstract This study investigates the problem of areostationary orbits around Mars in three-dimensional space. Areostationary orbits are expected to be used to establish a future telecommunication network for the exploration of Mars. However, no artificial satellites have been placed in these orbits thus far. The characteristics of the Martian gravity field are presented, and areostationary points and their linear stability are calculated. By taking linearized solutions in the planar case as the initial guesses and utilizing the Levenberg-Marquardt method, families of periodic orbits around areostationary points are shown to exist. Short-period orbits and long-period orbits are found around linearly stable areostationary points, but only short-period orbits are found around unstable areostationary points. Vertical periodic orbits around both linearly stable and unstable areostationary points are also examined. Satellites in these periodic orbits could depart from areostationary points by a few degrees in longitude, which would facilitate observation of the Martian topography. Based on the eigenvalues of the monodromy matrix, the evolution of the stability index of periodic orbits is determined. Finally, heteroclinic orbits connecting the two unstable areostationary points are found, providing the possibility for orbital transfer with minimal energy consumption.

Key words: planets and satellites: Mars — martian gravity field — periodic orbit — areostationary orbits

1 INTRODUCTION

Stationary orbits are approximately equatorial and circular, and share the same period as the planetary rotation. Satellites in stationary orbits remain in orbit over the same location on the planetary surface. The notion of stationary orbits for Earth was first proposed by Clarke, and these orbits were considered to be a good application for communication satellites (Clarke 1945). Earth's geostationary orbits have been widely used in practical engineering applications, including communication, navigation, and meteorological applications. Geostationary orbits have been studied for many years, and plenty of papers have contributed to this research.

Stationary orbits around Mars are also known as areostationary orbits, and their characteristics are similar to Earth's geostationary orbits. Areostationary orbits are expected to be used to establish

* Supported by the National Natural Science Foundation of China.

future telecommunication networks for the exploration of Mars (Edwards et al. 2000; Bell et al. 2000; Hastrup et al. 2003; Turner 2006; Edwards & Depaula 2007; Edwards 2007). However, no artificial satellites have been placed in these orbits thus far, and few studies concerning stationary orbits around Mars have been conducted.

The positions of stationary points of Earth, the Moon, and Mars were found to be singular points of the zero-velocity surface (Zhuravlev 1977). For Earth and Mars, Deprit and López-Moratalla proved that the two linearly stable points are also stable in the sense of Liapunov properties (Deprit & López-Moratalla 1996). The influences of the individual harmonics of the Martian potential on the positions of stationary points were examined qualitatively and quantitatively, in which the C_{20}, C_{22}, and S_{22} terms were considered in the planar case (Wytrzyszczak 1998). In other research on areostationary orbits, the drift in longitude due to spherical harmonics up to the second degree and order was analyzed, and both the period of libration and the amount of stationkeeping maneuvers were calculated (Alvarellos 2011). Liu et al. also analyzed the longitudinal drift in the Martian second degree and order gravity field, and more accurate stationary points for reducing drift in the full gravity field were obtained using numerical methods (Liu et al. 2010). In addition, periodic orbits around equilibrium points in the Earth second degree and order gravity field (Lara & Elipe 2002) and in an arbitrary second degree and order uniformly rotating gravity field (Hu & Scheeres 2008) have been studied in terms of planar motion.

This paper investigates areostationary orbits in three-dimensional space. The major perturbation of concern is the effect of the Martian gravity field, and the ways in which the gravitational potential of Mars independently influences areostationary orbits are explored. The results can be used as a starting point for correction methods when considering all the perturbations including three-body perturbations, atmospheric forces, and solar radiation pressure. By taking linearized solutions in the planar case as the initial guesses and utilizing the Levenberg-Marquardt method (Levenberg 1944; Marquardt 1963; Moré 1977), it is demonstrated that periodic orbits exist around both unstable and linearly stable areostationary points, and their stability indexes are also calculated. Finally, heteroclinic orbits connecting the two unstable areostationary points are found, providing the possibility for orbital transfer with minimal fuel expenditure.

2 THE MARTIAN GRAVITY FIELD

The gravitational potential U in the body-fixed reference frame is expressed as follows (Kaula 1966)

$$U = \frac{\mu}{r}\left[1 + \sum_{l=1}^{\infty}\sum_{m=0}^{l}\left(\frac{R_{\mathrm{e}}}{r}\right)^{l} P_{lm}\left(\sin\varphi\right)\left(C_{lm}\cos m\lambda + S_{lm}\sin m\lambda\right)\right], \tag{1}$$

where μ is the Martian gravitational constant; R_{e} is the reference radius of Mars; r is the position of the spacecraft; P_{lm} is the associated Legendre function of degree l and order m; C_{lm} and S_{lm} are the coefficients of the spherical harmonic expansion; ϕ is the latitude of the body-fixed coordinate system; and λ is the longitude of the body-fixed coordinate system. For Mars, the prime meridian is defined as the longitude of the crater Airy-0.

The recently improved spherical harmonic Martian gravity field used in this paper is MRO110B2 (Konopliv et al. 2011). The values of some first coefficients of MRO110B2 are given in Table 1. The gravity coefficients are normalized and are related to the unnormalized coefficients as follows (Kaula 1966)

$$\begin{pmatrix} C_{lm} \\ S_{lm} \end{pmatrix} = \left[\frac{(l-m)!\,(2l+1)\,(2-\delta_{0m})}{(l+m)!}\right]^{1/2} \begin{pmatrix} \bar{C}_{lm} \\ \bar{S}_{lm} \end{pmatrix}, \tag{2}$$

where δ_{0m} is the Kronecker delta

$$\delta_{0m} = \begin{cases} 1, & \text{if } m = 0, \\ 0, & \text{if } m \neq 0. \end{cases} \tag{3}$$

Table 1 Normalized values of certain normalized zonals and tesserals of the Martian gravity model MRO110B2.

l	m	$\bar{C}_{lm}$	$\bar{S}_{lm}$
2	0	–0.8750219729111999E–03	0
2	2	–0.8463591454722000E–04	0.4893448966831000E-04
3	0	–0.1189641481101000E–04	0
3	2	–0.1594791937546000E–04	0.8361425579193003E–05

The value of the reference radius R_e = 3 396 000 m, and the value of the gravitational constant μ = 4.2828374527$\times 10^{13}$ m^3 s^{-2} (Konopliv et al. 2011).

It is well known that the gravity field of Mars is farther away from the potential of a sphere than that of Earth (Wytrzyszczak 1998); therefore, areostationary orbits are more perturbed than geostationary orbits. According to the Martian gravity field MRO110B2, it is obvious that the Martian oblateness term C_{20} is dominant among all harmonic coefficients, but it is not as dominant as Earth's C_{20}. The Martian C_{30} term has the opposite sign and is stronger compared to Earth's C_{30}. Moreover, the Martian tesseral harmonics are also stronger than those of Earth. Unlike Earth, the Martian C_{22} and S_{22} terms have different signs.

Previous research has determined that the terms C_{20}, C_{22}, S_{22}, C_{30}, C_{32}, and S_{32} are essential for areostationary orbits (Wytrzyszczak 1998). The zonal harmonic C_{20} causes the main shift of the position of areostationary points in the radial direction; the tesseral harmonics C_{22} and S_{22} mainly influence the longitudinal distribution of areostationary points and the distances of areostationary points from Mars; the terms C_{30}, C_{32}, and S_{32} contribute significantly to the displacement in the z direction; and other harmonics only result in invisible changes in the position of areostationary points. The gravitational potential U including these essential terms is written as follows

$$\begin{aligned} U = \frac{\mu}{r}\Big[1 + \frac{C_{20}R_e^2}{2r^2}\left(3\sin^2\varphi - 1\right) + \frac{3R_e^2}{r^2}\cos^2\varphi\left(C_{22}\cos 2\lambda + S_{22}\sin 2\lambda\right) \\ + \frac{C_{30}R_e^3}{2r^3}\left(5\sin^3\varphi - 3\sin\varphi\right) + \frac{15R_e^3}{r^3}\sin\varphi\cos^2\varphi\left(C_{32}\cos 3\lambda + S_{32}\sin 3\lambda\right)\Big]. \end{aligned} \tag{4}$$

3 EQUATIONS OF MOTION

The motion of a satellite can be described in a rotating reference frame that is rotating with Mars. Accordingly, the rotating reference frame *Oxyz* is established with the origin O located at the center of mass of Mars, the z-axis taken as the rotation axis, and the x-axis coinciding with the prime meridian. It is assumed that Mars rotates uniformly around the z-axis with constant angular velocity ω. Equation (4) can be rewritten in the form of rectangular Cartesian coordinates as follows

$$\begin{aligned} U = \frac{\mu}{r} - \frac{\mu R_e^2 C_2\left(x^2+y^2-2z^2\right)}{2r^5} + \frac{3\mu R_e^2 C_{22}\left(x^2-y^2\right)}{r^5} \\ + \frac{6\mu R_e^2 S_{22}xy}{r^5} + \frac{15\mu R_e^3 C_{32}\left(x^2-y^2\right)z}{r^7} + \frac{30\mu R_e^3 S_{32}xyz}{r^7}. \end{aligned} \tag{5}$$

In mechanics, the effective potential W is defined as the combined gravitational potential and rotational potential terms as follows (Scheeres et al. 2002; Thomas 1993)

$$W = \frac{1}{2}\omega^2\left(x^2 + y^2\right) + U. \tag{6}$$

Then, the Lagrangian L of the motion is expressed as

$$L = \frac{1}{2}\left(\dot{x}^2 + \dot{y}^2 + \dot{z}^2\right) + \omega\left(x\dot{y} - \dot{x}y\right) + \frac{1}{2}\omega^2\left(x^2 + y^2\right) + U, \tag{7}$$

where T is the kinetic energy. Scaling is performed so that $l = \left(\mu/\omega^2\right)^{1/3}$ is the unit of length and $1/\omega$ is the unit of time. With scaling, the Lagrangian L is rewritten as

$$L = \frac{1}{2}\left(\dot{x}^2 + \dot{y}^2 + \dot{z}^2\right) + (x\dot{y} - \dot{x}y) + \frac{1}{2}\left(x^2 + y^2\right) + V, \tag{8}$$

where $V = U/\left(\omega^2 l^2\right)$. It is obvious that the Lagrangian is time-invariant, so the dynamical system admits the Jacobian integral J as follows

$$J = \frac{1}{2}\left(\dot{x}^2 + \dot{y}^2 + \dot{z}^2\right) - \frac{1}{2}\left(x^2 + y^2\right) - V. \tag{9}$$

The Lagrange equations are written as

$$\frac{d}{dt}\left(\frac{\partial L}{\partial \dot{r}}\right) - \frac{\partial L}{\partial r} = 0. \tag{10}$$

Therefore, the equations of motion of the spacecraft in the rotating reference frame *Oxyz* can be written as

$$\begin{aligned} &\ddot{x} - 2\dot{y} = x + V_x, \\ &\ddot{y} + 2\dot{x} = y + V_y, \\ &\ddot{z} = V_z. \end{aligned} \tag{11}$$

4 AREOSTATIONARY POINTS

Areostationary points can be located by setting the right-hand sides of Equation (11) to zero, i.e.

$$\begin{aligned} &x + V_x = 0\,, \\ &y + V_y = 0\,, \\ &V_z = 0\,. \end{aligned} \tag{12}$$

The initial values of the areostationary points are chosen from Liu et al. (2010). With these initial values, the Levenberg-Marquardt method (Levenberg 1944; Marquardt 1963; Moré 1977) based on nonlinear least-squares algorithms can be applied to solve the nonlinear Equation (12). The iteration is processed until the tolerance of Equation (12) is less than 10^{-13}. Finally, the positions of the areostationary points can be obtained, which are shown in Table 2.

Table 2 Positions of Areostationary Points in the Rotating Frame

Areostationary Point	x	y	z	Linear Stability*
E_1	–0.965866684631854	0.259123824182275	–0.000000206550979	LS
E_2	0.259126533910926	0.965876790581445	0.000000640235545	U
E_3	0.965866684631854	–0.259123824182275	–0.000000206550979	LS
E_4	–0.259126533910926	–0.965876790581445	0.000000640235545	U

Notes: * LS = linearly stable; U = unstable.

5 THE LINEAR STABILITY OF AREOSTATIONARY POINTS

The linear stability of areostationary points can be determined by analyzing the linearized equations of the system represented by Equation (11) in the vicinity of areostationary points. Because of the symmetry of the system, the stabilities of areostationary points E_1 and E_3 are identical, and the stabilities of areostationary points E_2 and E_4 are identical.

Using the notation

$$\xi = x - x_e, \qquad \eta = y - y_e, \qquad \gamma = z - z_e, \tag{13}$$

and

$$\boldsymbol{X}\left(t\right)=\left(\xi,\ \eta,\ \gamma,\ \dot{\xi},\ \dot{\eta},\ \dot{\gamma}\right)^{\mathrm{T}}, \tag{14}$$

where x_e, y_e, and z_e are the coordinates of the areostationary point, the linearized equations of the system represented by Equation (11) can be expressed as

$$\dot{\boldsymbol{X}}\left(t\right)=\boldsymbol{A}\left(t\right)\cdot\boldsymbol{X}\left(t\right), \tag{15}$$

where

$$\boldsymbol{A}\left(t\right)=\begin{bmatrix}0 & 0 & 0 & 1 & 0 & 0\\ 0 & 0 & 0 & 0 & 1 & 0\\ 0 & 0 & 0 & 0 & 0 & 1\\ W_{xx} & W_{xy} & W_{xz} & 0 & 2\omega & 0\\ W_{yx} & W_{yy} & W_{yz} & -2\omega & 0 & 0\\ W_{zx} & W_{zy} & W_{zz} & 0 & 0 & 0\end{bmatrix}. \tag{16}$$

The second order partial derivatives of the effective potential $\nabla\nabla W$ must be calculated at the corresponding areostationary point.

For areostationary points E_1 and E_3, the six eigenvalues of the matrix $\boldsymbol{A}(t)$ are calculated as

$$\begin{aligned}&\lambda_{1,2}=\pm0.007924462675369\,i, \qquad \lambda_{3,4}=\pm0.999892722423221\,i,\\ &\lambda_{5,6}=\pm1.000075870390122\,i.\end{aligned} \tag{17}$$

They are all purely imaginary, so areostationary points E_1 and E_3 are linearly stable. For areostationary points E_2 and E_4, the six eigenvalues of the matrix $\boldsymbol{A}(t)$ are calculated as

$$\begin{aligned}&\lambda'_{1,2}=\pm0.007923923801517, \qquad \lambda'_{3,4}=\pm0.999945057867454\,i,\\ &\lambda'_{5,6}=\pm1.000086331179820\,i.\end{aligned} \tag{18}$$

Since $\lambda'_1>0$, areostationary points E_2 and E_4 are unstable. The states of stability of all these areostationary points appear in the fifth column of Table 2.

6 PERIODIC ORBITS AROUND AREOSTATIONARY POINTS

Note that around areostationary points, the displacement in the z direction is much smaller than that in the x or y direction. The periodic orbits of the linearized system represented by Equation (15) in the *xy*-plane can be obtained easily. Therefore, the linearized periodic solutions in the *xy*-plane can be taken as the initial guesses of periodic orbits around areostationary points in the three-dimensional space.

6.1 Short-period Orbits around Linearly Stable Areostationary Points

The motion of the spacecraft in the *xy*-plane corresponds to the case of C_{30} = 0, C_{32}= 0, S_{32}= 0, and z= 0. Around areostationary points E_1 and E_3, the general solutions of the linearized system represented by Equation (15) in the xy-plane are

$$\begin{aligned}&\xi=A_1\sin\left(\kappa_1 t+\varphi_1\right)+A_2\sin\left(\kappa_2 t+\varphi_2\right),\\ &\eta=\alpha A_1\cos\left(\kappa_1 t+\varphi_1\right)+\alpha A_2\cos\left(\kappa_2 t+\varphi_2\right),\end{aligned} \tag{19}$$

where κ_1 and κ_2 are the frequencies; A_1 and A_2 are the amplitudes; and $\alpha=\frac{1}{2}\left(\kappa_2+W_{xx}/\kappa_2\right)$. Since $\kappa_2\ll\kappa_1$, the general solutions of the linearized system in the *xy*-plane consist of long-period and short-period terms.

Here, only the case of E_1 is considered because the cases of E_1 and E_3 are symmetrical. First, set $A_1\neq0$ and A_2 = 0; thus, only short-period terms are retained

$$\xi=A_1\sin\left(\kappa_1 t+\varphi_1\right), \qquad \eta=\alpha A_1\cos\left(\kappa_1 t+\varphi_1\right). \tag{20}$$

The motion of the spacecraft is approximately periodic with period

$$T_0 = 2\pi/\kappa_1 \,. \tag{21}$$

For example, given amplitude A_1 = 0.01, the approximate periodic condition in the xy-plane is

$$\begin{array}{l} x_0 = -0.975525140963676\,,\ y_0 = 0.261715005628121\,,\ z_0 = 0\,, \\ \dot{x}_0 = 0.005182255008665\,,\quad \dot{y}_0 = 0.019316508183033,\ \dot{z}_0 = 0\,, \\ T = 6.283859422887580\,. \end{array} \tag{22}$$

Based on the above initial guess, the Levenberg-Marquardt method is used to solve the periodic condition

$$\begin{array}{l} r\left(t_0\right) - r\left(t_0 + T\right) = 0, \\ v\left(t_0\right) - v\left(t_0 + T\right) = 0. \end{array} \tag{23}$$

The iteration is processed until the mismatch between the position and velocity at the initial time t_0 and the position and velocity at the final time $t_0 + T$ is less than 10^{-12}. The exact initial condition of the periodic orbit is derived as

$$\begin{array}{l} x_0 = -0.975525140963676,\ y_0 = 0.261715005628121,\ z_0 = 0.000011183843109, \\ \dot{x}_0 = 0.005169425044549\,,\quad \dot{y}_0 = 0.019268683278553,\ \dot{z}_0 = 0.000001892841807\ , \\ T = 6.283859507415385. \end{array} \tag{24}$$

The periodic orbit around E_1 derived above is shown in Figure 1; it has an oval shape with a period of approximately 1.03 days. In this orbit, a spacecraft can depart from the areostationary point E_1 by about 1.15° at most in longitude. It is expected that useful multi-view images could be derived from an offset of a few degrees, especially for observations of Elysium Planitia and Iani Chaos below the stable areostationary points E_1 and E_3, respectively.

The family of short-period orbits is shown in Figure 2. It can be seen that the shape of the short-period orbits around E_1 changes from oval to heart-shaped as amplitude increases.

According to the theory of ordinary differential equations (Robinson 2004), the fundamental solution matrix $\boldsymbol{\Phi}(t)$ yields the following

$$\dot{\boldsymbol{\Phi}}\left(t\right) = \boldsymbol{A}\left(t\right)\boldsymbol{\Phi}\left(t\right). \tag{25}$$

The stability of periodic orbits can be determined by analyzing the eigenvalues of the monodromy matrix $\boldsymbol{\Phi}(T)$, where T is the motion's period. The monodromy matrix here is the product

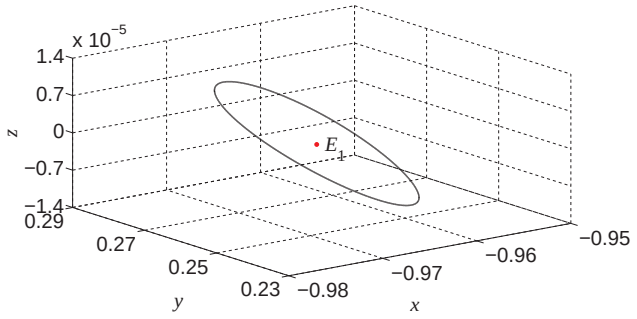

Fig. 1 Short-period oval-shaped orbit around the areostationary point E_1. Different scales are used for abscissas and ordinates.

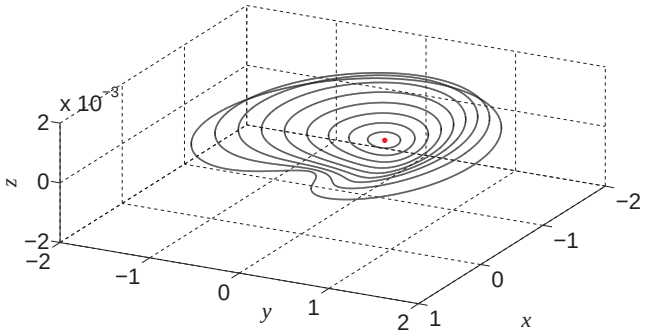

Fig. 2 Family of short-period orbits around the areostationary point E_1.

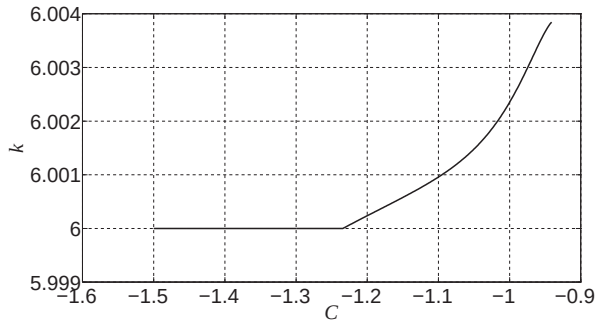

Fig. 3 Evolution of stability index k as a function of the Jacobian constant C for short-period orbits around E_1.

of the inverse of the fundamental matrix of Equation (11) evaluated at the zero and the fundamental matrix of Equation (11) evaluated at the period. The initial condition $\mathbf{\Phi}(0)$ used for the integration of Equation (25) is the identity matrix. For Hamiltonian systems, the eigenvalues of $\mathbf{\Phi}(T)$ come in pairs. Each pair is a reciprocal of the other. Thus, if one pair consists of two conjugate complex eigenvalues, both eigenvalues are on the unit circle, i.e. their modului are both equal to one.

Here, the stability index k is introduced to estimate the stability of the orbit, and is defined as the sum of all the eigenvalues of $\mathbf{\Phi}(T)$

$$k = \sum_{i=1}^{6} |\chi_i|, \tag{26}$$

where χ_i is the eigenvalue of $\mathbf{\Phi}(T)$. Therefore, if $k > 6$, the orbit is unstable; if $k = 6$, the orbit is stable.

The general behavior of the stability index k as a function of the Jacobian constant is presented in Figure 3. It can be seen that the E_1 family of periodic orbits changes from stable ($k = 6$) to unstable ($k > 6$) as the value of the Jacobian constant increases.

6.2 Long-period Orbits around Linearly Stable Areostationary Points

When $A_1 = 0$ and $A_2 \neq 0$, only long-period terms are retained

$$\xi = A_2 \sin(\kappa_2 t + \varphi_2) \ , \qquad \eta = \alpha A_2 \cos(\kappa_2 t + \varphi_2) \ . \tag{27}$$

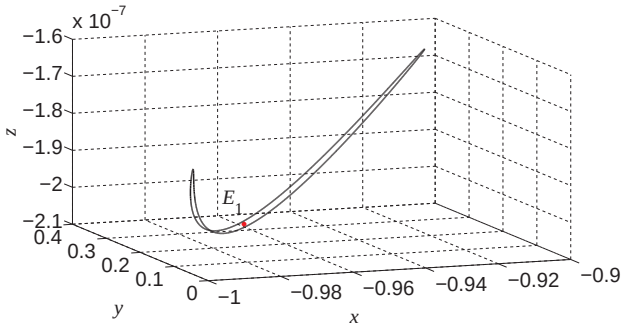

Fig. 4 Long-period orbit around the areostationary point E_1.

If A_1= 0 and A_2 = 0.001, Equation (27) is taken as the initial guess, and the Levenberg-Marquardt method is utilized until the mismatch between the position and velocity at the initial time t_0 and the position and velocity at the final time $t_0 + T$ is less than 10^{-13}. Then, the exact parameters for the periodic orbit can be obtained as

$$\begin{aligned} &x_0 = -0.966832530336112\,,\ y_0 = 0.259382942061755\,,\ z_0 = -0.000000206142371\,,\\ &\dot{x}_0 = 0.000388605225698\,,\quad \dot{y}_0 = 0.001448499930975\,,\ \dot{z}_0 = 0.000000000052347\,,\\ &T = 800.1262797809567\,. \end{aligned} \tag{28}$$

The long-period orbit around the areostationary point E_1 is shown in Figure 4. The period of the orbit is approximately 0.36 years. For this long-period orbit, the six eigenvalues of the monodromy matrix $\boldsymbol{\Phi}(T)$ are all on the unit circle, and it is easy to see that k= 6, based on Equation (26). Thus, this long-period orbit around the areostationary point E_1 is stable.

6.3 Short-period Orbits around Unstable Areostationary Points

Around areostationary points E_2 and E_4, the general solutions of the linearized system represented by Equation (15) in the *xy*-plane are

$$\begin{aligned} &\xi = D_1 \mathrm{e}^{\kappa_1' t} + D_2 \mathrm{e}^{-\kappa_1' t} + A' \sin\left(\kappa_2' t + \varphi'\right),\\ &\eta = \alpha_1' \left(D_1 \mathrm{e}^{\kappa_1' t} - D_2 \mathrm{e}^{-\kappa_1' t}\right) + \alpha_2' A' \cos\left(\kappa_2' t + \varphi'\right), \end{aligned} \tag{29}$$

where κ_1' and κ_2' are the frequencies; D_1, D_2, and A' are the amplitudes; and $\alpha_1' = \frac{1}{2}\left(\kappa_1' - W_{xx}/\kappa_1'\right)$ and $\alpha_2' = \frac{1}{2}\left(\kappa_2' + W_{xx}/\kappa_2'\right)$. It can be seen that Equation (29) consists of secular terms, attenuation terms, and periodic terms. In order to derive periodic orbits, the coefficient of secular term D_1 and the coefficient of attenuation term D_2 must be set equal to zero, so

$$\xi = A' \sin\left(\kappa_2' t + \varphi'\right), \qquad \eta = \alpha_2' A' \cos\left(\kappa_2' t + \varphi'\right). \tag{30}$$

Based on the Levenberg-Marquardt method, the initial guess of the periodic orbit represented by Equation (30) can be slightly adjusted. The iteration is processed until the mismatch between the position and velocity at the initial time t_0 and the position and velocity at the final time $t_0 + T$ is less than 10^{-12}. Taking the case of $A' = 0.01$ as an example, the exact initial parameters for the periodic orbit can be obtained as

$$\begin{aligned} &x_0 = \ 0.261717716762586,\ \ y_0 = 0.975535246535669,\ \ z_0 = -\,0.000045126967204,\\ &\dot{x}_0 = \ 0.019269493269170,\ \ \dot{y}_0 = 0.005169641770384,\ \ \dot{z}_0 = \ -\,0.000002453663158,\\ &T = \ \ 6.283530658585495. \end{aligned} \tag{31}$$

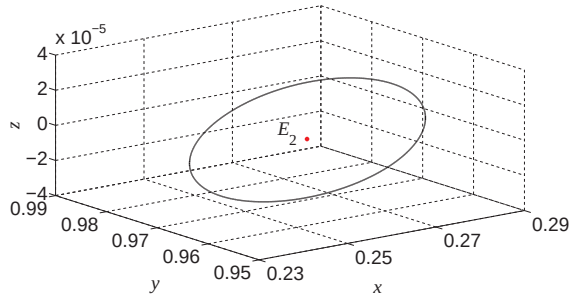

Fig. 5 Oval-shaped periodic orbit around the unstable areostationary point E_2.

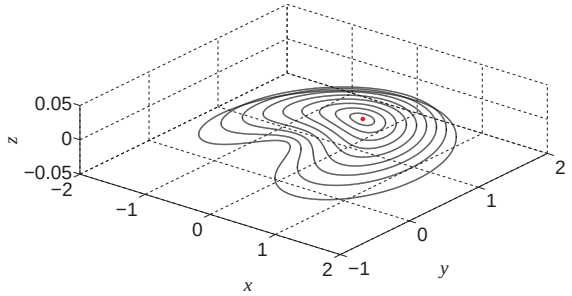

Fig. 6 Family of short-period orbits around the areostationary point E_2.

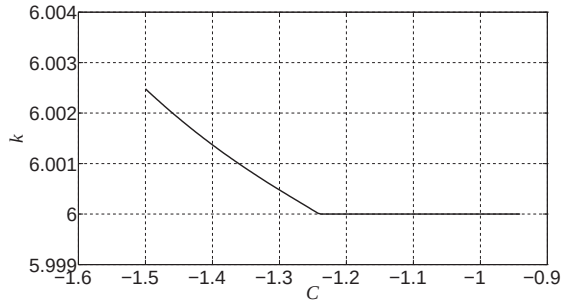

Fig. 7 Evolution of the stability index k as a function of the Jacobian constant C for short-period orbits around E_2.

An oval-shaped periodic orbit around the areostationary point E_2 is shown in Figure 5; its period is approximately 1.03 days.

Figure 6 shows that the shapes of the periodic orbits around E_2 also change from oval to heart-shaped as amplitude increases.

Figure 7 presents the evolution of the stability index k as a function of the Jacobian constant. It is clear that the E_2 family of periodic orbits changes from unstable ($k > 6$) to stable ($k = 6$) as the value of the Jacobian constant increases. It can be seen that stable periodic orbits exist around unstable areostationary points. This means that a spacecraft could stay in the vicinity of an unstable areostationary point for a long time, which would facilitate observation of Martian topography, including Syrtis Major Planum and Tharsis below unstable areostationary points E_2 and E_4, respectively.

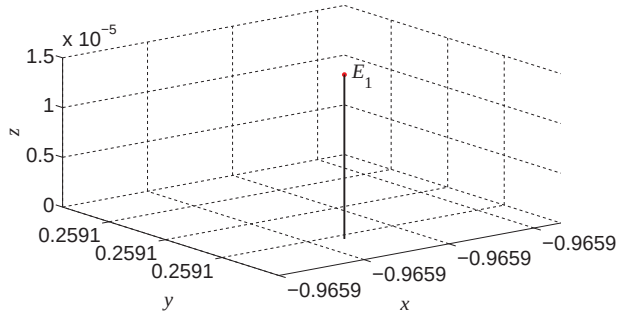

Fig. 8 Vertical periodic orbit around the linearly stable areostationary point E_1.

6.4 Vertical Period Orbits around both Linearly Stable and Unstable Areostationary Points

Vertical periodic orbits around both linearly stable and unstable areostationary points are also noted, which are different from both short-period and long-period orbits. The motion of the spacecraft in the z direction corresponds to the case of $\xi = 0$ and $\eta = 0$.

Around all areostationary points, it is easy to obtain that the eigenvalues of Equation (15) in the z direction are all purely imaginary. Thus, the general solutions of the linearized system represented by Equation (15) in the z direction are calculated as

$$\gamma = B\sin(\varsigma t + \theta), \tag{32}$$

where ς is the frequency, and B is the amplitude. Based on the initial guess represented by Equation (32), the periodic character (23) can be confirmed using the Levenberg-Marquardt method. The iteration is processed until the mismatch between the position and velocity at the initial time t_0 and the position and velocity at the final time $t_0 + T$ is less than 10^{-12}.

For example, given the amplitude A= 10^{-5} around the areostationary point E_1, the exact initial parameters for the vertical periodic orbit can be obtained as

$$\begin{array}{lll} x_0 = -0.965866684631854, & y_0 = 0.259123824182275, & z_0 = 0.000008038019607, \\ \dot{x}_0 = 0, & \dot{y}_0 = 0, & \dot{z}_0 = 0.000000506705147, \\ T = 6.282708621687184. & & \end{array} \tag{33}$$

The vertical periodic orbit around E_1 derived above is shown in Figure 8; its period is approximately 1.03 days. For this vertical periodic orbit, the six eigenvalues of the monodromy matrix $\mathbf{\Phi}(T)$ are all on the unit circle, and it is easy to see that $k = 6$, based on Equation (26). Thus, this vertical periodic orbit around the linearly stable areostationary point E_1 is stable.

Given amplitude $A = 10^{-5}$ around the areostationary point E_2, the exact initial parameters for the vertical periodic orbit can be obtained as

$$\begin{array}{lll} x_0 = 0.259126533910926, & y_0 = 0.965876790581445, & z_0 = 0.000008320016725, \\ \dot{x}_0 = 0, & \dot{y}_0 = 0, & \dot{z}_0 = 0.000001413345788, \\ T = 6.282642913717483. & & \end{array} \tag{34}$$

The vertical periodic orbit around E_2 derived above is shown in Figure 9; its period is also approximately 1.03 days. For this vertical periodic orbit, it is easy to obtain that $k = 6.0025$ based on Equation (26). Thus, this vertical periodic orbit around the unstable areostationary point E_2 is unstable. Note that the vertical periodic orbits around areostationary points E_1 and E_2 are both below the areostationary points.

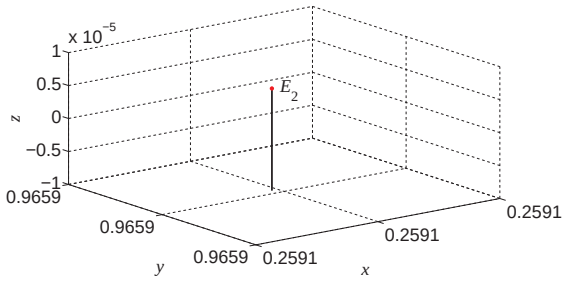

Fig. 9 Vertical periodic orbit around the unstable areostationary point E_2.

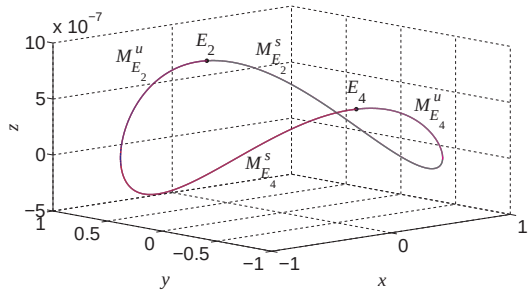

Fig. 10 Heteroclinic orbits connecting unstable areostationary points E_2 and E_4. The red line corresponds to the unstable manifold of E_2 (*color online*); the blue line corresponds to the stable manifold of E_4; the pink line corresponds to the unstable manifold of E_4; and the green line corresponds to the stable manifold of E_2.

7 HETEROCLINIC ORBITS CONNECTING THE TWO UNSTABLE AREOSTATIONARY POINTS

The numerical method used to calculate the stable and unstable manifolds in this study was developed in previous research (Robinson 2004). The local stable and unstable manifolds of areostationary points are approximated with line segments through the areostationary points in the directions of stable eigenvector ν^s and unstable eigenvector ν^u; these eigenvectors can be obtained easily by analyzing the linearized equation in the vicinity of the areostationary point. Take the calculation of the unstable manifold of the areostationary point E_2 as an example. For a sufficiently small δ (given as 10^{-9} here), a point X in the neighborhood of the areostationary point E_2 is selected so that

$$X = E_2 + \delta v^u. \tag{35}$$

Taking X as the initial value, the global unstable manifold can be obtained by integrating Equation (11) forward. Following a similar procedure, the global stable manifold can also be obtained by backward iteration.

Figure 10 illustrates the stable and unstable manifolds of areostationary points E_2 and E_4. Note that the unstable manifold $M^u_{E_2}$ of E_2 coincides with the stable manifold $M^s_{E_4}$ of E_4, which is known as the heteroclinic orbit connecting unstable areostationary points E_2 and E_4. It can also be seen that the unstable manifold $M^u_{E_4}$ of E_4 coincides with stable manifold $M^s_{E_2}$ of E_2, which is another heteroclinic orbit connecting E_2 and E_4. The existence of heteroclinic orbits means that a spacecraft at the unstable areostationary point could transfer to another unstable areostationary point with minimal energy consumption.

8 CONCLUSIONS

This study analyzes areostationary orbits around Mars in three-dimensional space. Areostationary points are derived in the rotating reference frame, and it is shown that periodic orbits exist around both linearly stable and unstable areostationary points. For short-period orbits around linearly stable areostationary points, their stabilities evolve from stable to unstable as the Jacobian constant increases. For short-period orbits around unstable areostationary points, their stabilities evolve from unstable to stable as the Jacobian constant increases. It is also determined that vertical periodic orbits around linearly stable areostationary points are stable, while vertical periodic orbits around unstable areostationary points are unstable. Finally, heteroclinic orbits connecting the two unstable areostationary points are found, providing the possibility for orbital transfer with minimal fuel expenditure.

Acknowledgements This work was supported by the National Basic Research Program of China (973 Program, No. 2012CB720000) and the National Natural Science Foundation of China (Grant No. 11072122).

References

Alvarellos, J. L. 2011, The Journal of the Astronautical Sciences, 57

Anderson, R., Bar-Sever, Y., Bell, D., Ely, T., Guinn, J., Hart, M., Kallemeyn, P., Levene, E., Jah, M., Romans, L., & Wu, S. 1999, in International Symposium on Space Communications and Navigation Technologies (Pasadena, California)

Bell, D. J., Cesarone, R. J., Ely, T. A., Edwards, C. D., & Townes, S. A. 2000, in IEEE Aerospace Conference Proceedings, 7 (Big Sky, MT), 75

Clarke, A. C. 1945, Wireless World, 11, 305

Deprit, A., & López-Moratalla, T. 1996, Revista Matemática Universidad Complutense, 9, 311

Edwards, C. D. 2007, International Journal of Satellite Communications and Networking, 25, 111

Edwards, C. D., Adams, J. T., Agre, J. R., et al. 2000, in Concepts and Approaches for Mars Exploration (Houston), ed. N. G. Barlow, 105

Edwards, C. D., & Depaula, R. 2007, Acta Astronautica, 61, 131

Hastrup, R. C., Bell, D. J., Cesarone, R. J., et al. 2003, Acta Astronautica, 52, 227

Hu, W.-D., & Scheeres, D. J. 2008, ChJAA (Chin. J. Astron. Astrophys.), 8, 108

Kaula, W. M. 1966, Theory of Satellite Geodesy: Applications Of Satellites to Geodesy (Waltham: Blaisdell)

Konopliv, A. S., Asmar, S. W., Folkner, W. M., et al. 2011, Icarus, 211, 401

Lara, M., & Elipe, A. 2002, Celestial Mechanics and Dynamical Astronomy, 82, 285

Levenberg, K. 1944, Quarterly of Applied Mathematics, 2, 164

Liu, X., Baoyin, H., & Ma, X. 2010, Journal of Guidance, Control, and Dynamics, 33, 1294

Marquardt, D. W. 1963, SIAM Journal Applied Mathematics, 11, 431,

Moré, J. J. 1977, in Lecture Notes in Mathematics 630: Numerical Analysis, ed., G. A. Watson (Dundee: Springer Verlag), 105

Robinson, R. C. 2004, An Introduction to Dynamical Systems: Continuous and Discrete (New Jersey: Prentice Hall)

Scheeres, D. J., Durda, D. D., & Geissler, P. E. 2002, Asteroids III, eds. W. F. Bottke et al. (Tucson: University of Arizona Press), 527

Turner, A. E. 2006, in 24th AIAA International Communications Satellite Systems Conference, AIAA-2006-5313 (San Diego, California), *http://www.aric.or.kr/treatise/journal/content.asp?idx=106088*

Thomas, P. C. 1993, Icarus, 105, 326

Wytrzyszczak, I. 1998, Artificial Satellites, 33, 11

Zhuravlev, S. G. 1977, AZh, 54, 909